Proceedings of the 9th U.S. National and 10th Canadian Conference on Earthquake Engineering
Compte Rendu de la 9ième Conférence Nationale Américaine et
10ième Conférence Canadienne de Génie Parasismique
July 25-29, 2010, Toronto, Ontario, Canada • Paper No 1636

EFFECT OF LONGITUDINAL REINFORCEMENT RATIO ON THE FAILURE MECHANISM OF R/C COLUMNS MOST VULNERABLE TO COLLAPSE

C. Woods[1] and A. B. Matamoros[2]

ABSTRACT

Models to calculate the drift ratio at axial load failure of reinforced concrete columns such as that proposed by Elwood and Moehle indicate that the drift ratio at axial load failure is primarily a function of axial load demand and the detailing of the transverse reinforcement. A series of column tests recently completed at the MAST facility at the University of Minnesota showed that for R/C columns most vulnerable to collapse the longitudinal reinforcement ratio had a very significant effect on the drift ratio at axial failure. Three full-scale experiments were carried out at the NEES-MAST facility at the University of Minnesota as part of a large study on the risk of collapse of older concrete buildings during major earthquakes. Tests evaluated the behavior of columns with ratios of nominal shear strength to plastic shear demand on the order of 0.85. The longitudinal and transverse reinforcement ratios were maintained constant, while the axial load ratio and the longitudinal reinforcement ratio were varied. Axial loads were 0.3 and 0.2 $f'_c A_g$, and the longitudinal reinforcement ratios were 2.5 and 3%. All columns had a height of 2945 mm and cross section of 457 x 457 mm. The transverse reinforcement consisted of No. 3 bars (9.5 mm diameter) spaced at a distance equivalent to the column size (457 mm). The loading protocol consisted of cycles with increasing maximum lateral displacement under constant axial load. The paper analyzes the load resisting mechanism and behavior of the specimens, and compares the experimental results with existing axial failure models and modeling and acceptance criteria in the ASCE-41 Standard.

Introduction

Recent efforts to improve our ability to evaluate the risk of collapse posed by older reinforced concrete buildings has led to the development of models to calculate the drift at axial failure of reinforced concrete columns. The tests described in this paper were carried out to gain a better understanding of the behavior of columns that pose the greatest risk of collapse.

Experimental Program

The experimental program consisted of three full-scale columns with square cross section. Columns (Fig. 1) were tested at the NEES-MAST Laboratory at the University of Minnesota (University of Minnesota, 2008). All specimens had a length of 2945 mm and cross

[1]Graduate Research Assistant, Dept. of Civil, Architectural, and Environmental Engineering, University of Kansas, Lawrence, KS 66045
[1]Associate Professor, Dept. of Civil, Architectural, and Environmental Engineering, University of Kansas, Lawrence, KS 66045

section dimensions of 457 x 457 mm, for a shear-span-to-depth ratio of 3.75. For columns 1 and 2 the longitudinal reinforcement consisted of 8 No. 9 bars (28.7 mm diameter) made of ASTM A706 steel with a measured yield strength of 445 MPa while for column 3 the longitudinal reinforcement consisted of 8 No. 10 bars (32.3 mm diameter) with a measured yield strength of 445 MPa. Transverse reinforcement consisted of No. 3 bars (9.5 mm diameter) made of ASTM A615 steel with a yield strength of 372 MPa. Transverse reinforcement consisted of closed hoops with 90 deg. bends spaced at 457 mm. Compressive strength of the concrete measured on the day of the test for specimens 1 and 2 was 33 MPa, and for specimen 3 was 17 MPa.

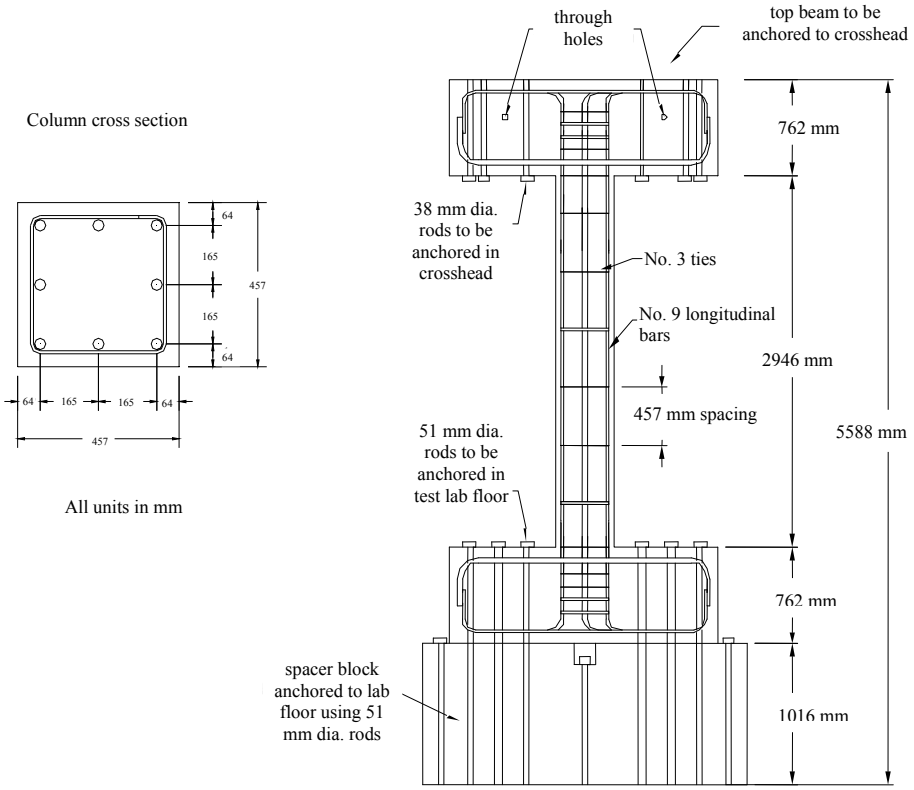

Figure 1 Specimen dimensions

Loading Protocol

Specimens were subjected to sets of three cycles with increasing displacement. The amplitude of each set of cycles was increased by 0.25% up to a drift ratio of 1.5%, and by 0.5% increments after that. Axial load remained constant with values of 2225 KN for specimens 1 and 3, and 1510 KN for specimen 2. These values correspond to axial load ratios of 0.32, 0.21, and 0.62 based on measured material properties.

The control system was configured to switch from load control to displacement control in the vertical actuators if a reduction in the axial load capacity was detected. The system was programmed to maintain the lateral and vertical deformation constant after the triggering criteria was met. This was designated as an axial failure event. After each failure event, the control

system was transitioned from displacement to load control in the axial direction, but under the reduced axial load recorded at the end of the failure event. After the axial load in the column was stabilized, the displacement protocol for the lateral deformation was continued. The loading protocol changed when damage to the columns was deemed too severe. At that point the vertical deformation was increased while maintaining the maximum lateral displacement recorded in the column constant. This was intended to obtain a measure of the residual axial capacity of the column.

The load protocol differs from similar tests reported in the literature (Sezen, 2000, Lynn 2001), in that instead finishing the test after the first axial failure event, lateral loading resumed under reduced axial load. One of the objectives of continuing the tests was to find out if the columns could stabilize at the same axial load after axial failure. This was of great significance to establish the threshold between columns that experience simultaneous shear and axial failure and columns that can maintain axial load after shear failure. Another objective was to learn about the lateral stiffness and residual axial load capacity of columns after axial failure. Field observations of heavily damaged buildings have shown that in some instances the floor system above the column is capable of redistributing part of the gravity loads to other elements of the vertical load system, primarily through catenary action of the beams and slab. Data such as that obtained in these tests may be used in the future to study if the loss of axial capacity in a column will lead to system or local collapse.

Shear Strength

The nominal shear strength of the column specimens calculated using various different methods is presented in Table 1. Shear strength provided by the concrete was calculated using expressions for V_c and V_{ci} in the 2008 edition of the ACI 318 Building Code (ACI Committee 318, 2008) and the ASCE-41 Standard (Elwood et al., 2007) and measured material properties. The nominal strength was calculated also based on the Modified Compression Field Theory, using the analysis program Response 2000 (Bentz and Collins, 2000). All methods indicated that the specimens were expected to fail due to shear soon after the appearance of flexural shear cracks. The nominal shear force expected to cause yielding of the flexural reinforcement (V_y in Table 1) was calculated based on a moment-curvature analysis. Calculated values of shear strength resulted in ratios of V_n to V_y ranging between 0.56 and 0.86, so the specimens were expected to fail in shear prior to yielding of the flexural reinforcement. Experimental results (Matchulat, 2008) showed that measured maximum lateral forces where almost identical to the nominal shear forced expected to cause yielding V_y.

Experimental Results

A profile of the measured deflections for column 3 is shown in Fig. 2a. The vertical lines show the calculated deflection at cracking and at yield. Deflection readings are consistent with measured shear values in that they indicate that the longitudinal bars of the specimen were very close to reaching the yield point in tension when axial failure took place. Recorded strain readings in the longitudinal reinforcement are shown in Fig. 3b. Strain gages labeled LM4 and RM4 were located at the top of the column, approximately 152 mm below the interface between the cap beam and the column. Both gages indicate that yielding of the longitudinal

reinforcement in tension did not occur prior to axial failure. However, readings show that both of the aforementioned gages experienced significant strains in compression, indicating that localized buckling likely occurred prior to axial failure. This is consistent with the large expansion of the core that was measured with displacement transducers, which came as a result of yielding of the transverse reinforcement and possibly anchorage failure of the hoops.

Table 1. Nominal Strength of Test Specimens

Col	N	V_{test}	V_{ci} [a]	V_c [b]	V_n [c]	V_n [d]	V_n [e]	V_n [f]	V_y	*Ratio of V_n/V_y*		
	KN	KN	KN	KN	KN	KN	KN	KN	KN	[c]	[d]	MCFT
1	2225	412	199	305	351	245	284	288	410	0.86	0.60	0.69
2	1510	361	154	264	311	201	254	324	360	0.86	0.56	0.71
3	2225	311	185	220	266	231	242	276	313	0.86	0.74	0.78

[a] Calculated according to ACI Eq. 11-10
[b] Calculated according to ACI Eq. 11-4
[c] V_c term according to ACI Eq. 11-4 and V_s term according to ACI Eq. 11-15
[d] V_c term according to ACI Eq. 11-10 and V_s term according to ACI Eq. 11-15
[e] Calculated using Modified Compression Field Theory
[f] Calculated using Eq. 6-4 of FEMA 356 and ASCE-41

Readings from strain gage LF5, located approximately 279 mm down from the interface between the column and the cap beam, are consistent with those of gages LM4 and RM4, although the magnitude of the compressive strains was significantly lower at this location. Measurements from gage LM7, located approximately 152 mm from the interface of the bottom beam and the column, suggest that the specimen was very close to reaching the yield point when axial failure took place.

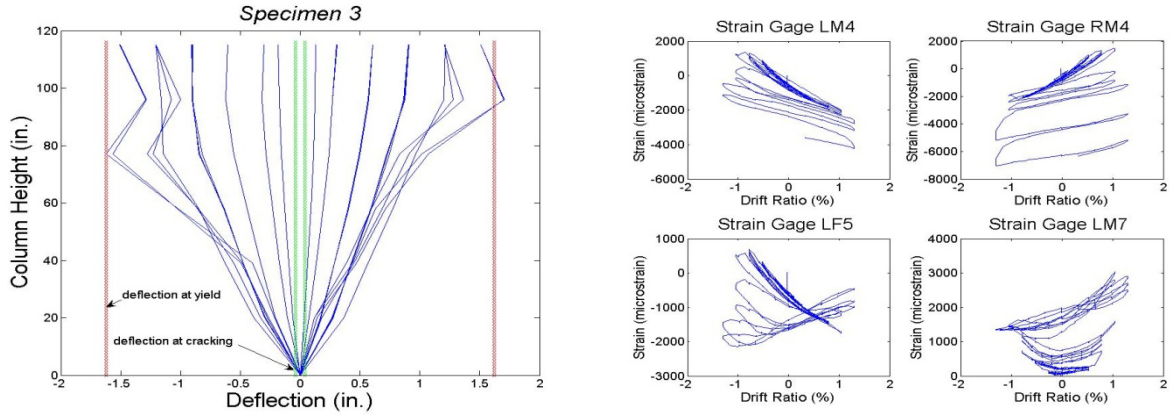

Figure 2. (a) Measured deflection profiles for column 3 (b) Recorded strains in longitudinal reinforcement for column 3.

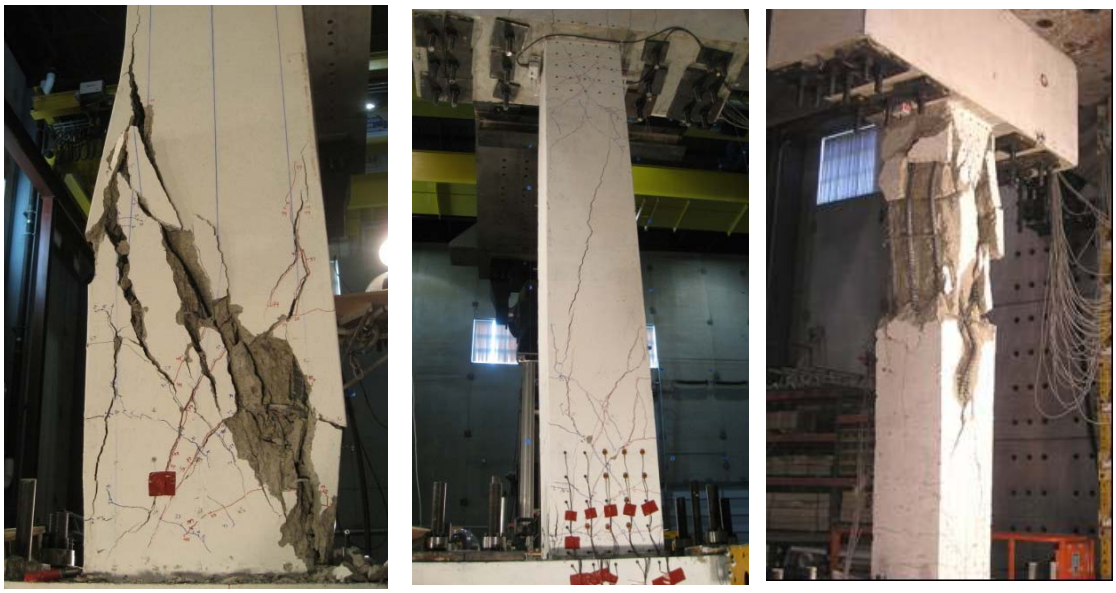

Figure 3. (a) Specimen 1 after axial failure (b) Specimen 2 after axial failure (c) Specimen 3 after axial failure

The behavior of all three specimens was very brittle in nature, although there were significant differences. For specimen 1 axial failure occurred at a drift ratio of 1.07%. Failure occurred after rapid widening of an existing shear crack (Fig. 3a and 3b), followed by sudden loss in axial capacity. The inclined crack associated with axial failure appeared in the maximum moment region, on the bottom side the specimen, and formed an angle of approximately 28 deg. with respect to the vertical axis of the column. Axial failure of column 2 was recorded at a drift ratio of 1.2% and it was precipitated by the appearance of an inclined crack in the middle section of the column (Fig. 3c). In the case of specimen 2 the crack formed a much shallower angle of approximately 14 deg. with respect to the vertical axis (Fig. 3c).

The behavior of column 3, with 3% longitudinal reinforcement ratio, was similar to that of specimen 2 up to the point of shear failure. A large shear crack (approximately 3 mm wide) formed through the center of the column at a drift ratio of approximately 1.07%. The angle of inclination of the crack with respect to the vertical column axis was observed to be approximately 13 deg. Although the appearance of this crack resulted in a significant reduction in the lateral stiffness of the column, the column was able to continue to sustain the full axial load of 2225 KN. A significant reduction in stiffness occurred from this point forward through the set of displacement cycles with a maximum drift ratio of 1.25%. Axial failure took place due to damage to the top maximum moment region of the column while unloading after the first positive peak, with the column reaching a maximum drift ratio of 1.6%.

Hysteresis curves for the three column specimens are presented in Fig. 4 a, b, and c. The darker line corresponds to the response prior to axial failure. The lighter line corresponds to the response after the first axial failure event. The dashed red line in Fig. 4 a, b and c, corresponds to the envelope curve according to ASCE-41 Supplement 1. The hysteretic response and sensor measurements (Matchulat, 2008) show that all three specimens failed prior to any significant yielding in flexure, and that the response was very brittle in nature. Although there was some

softening of the load displacement curve prior to the maximum lateral force, that may be attributed to the effect of inclined cracking. Figure 5 shows the effective shear modulus in the region of maximum moment as a function of the drift ratio for column 3. The effective shear modulus was calculated based on the measured lateral force and the deflection component related to shear, which was calculated using local deformations measured with an array of LED taggers placed in this area of the column.

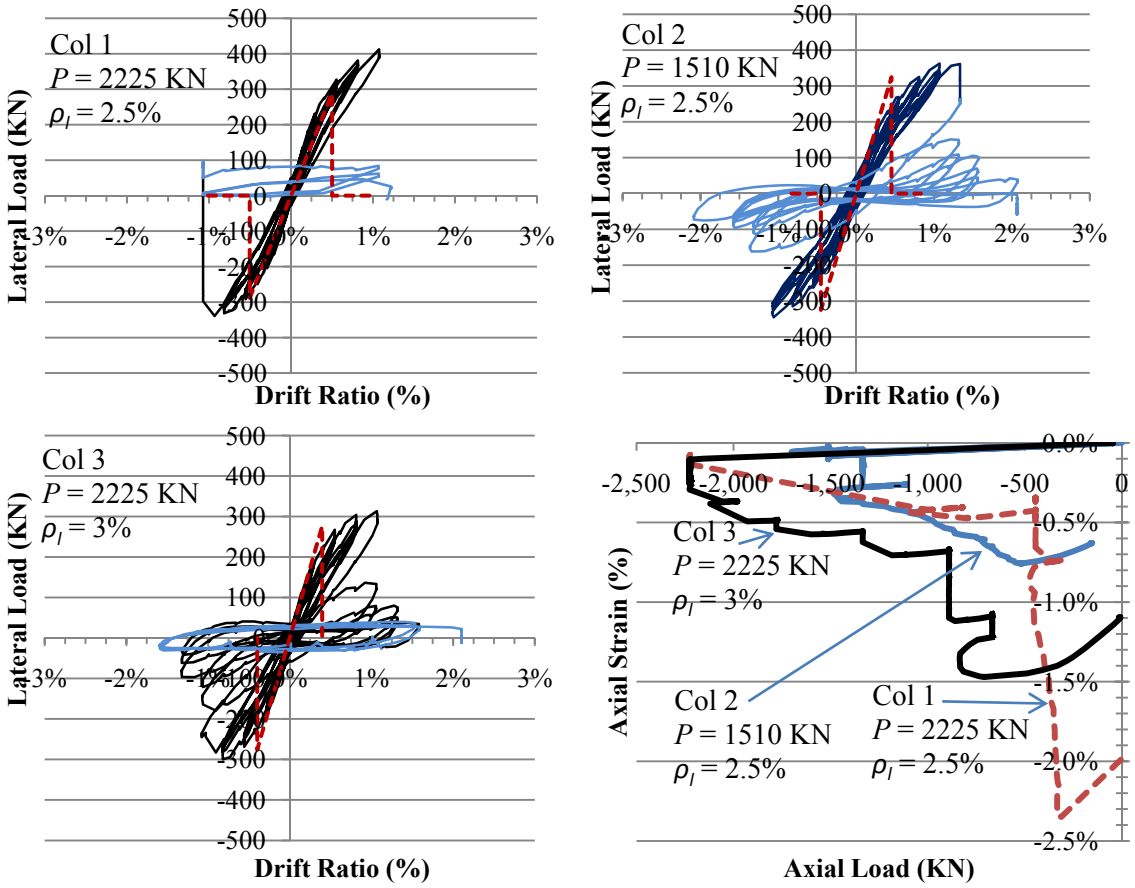

Figure 4. Load-Deflection relationship for (a) Column 1, (b) Column 2, (c) Column 3, (d) Axial Strain vs. Axial Load for all three columns

There were significant differences between the observed modes of failure, lateral stiffness, and residual strength of the three columns. Column 1, with the higher axial load and lower longitudinal reinforcement ratio (Fig. 4a) had the most brittle response. As previously indicated the column experienced simultaneous shear and axial failure. Subsequent cycles at lower axial load showed that combined failure caused the column to lose most of its lateral stiffness and axial load carrying capacity. The residual axial capacity of the column was approximately 500 KN which was very close to the axial capacity of the longitudinal reinforcement $A_s f_y$.

Shear failure for column 2 occurred at drift ratio of approximately 1.2%, with the appearance of a shear crack through the center of the column. The appearance of the shear crack

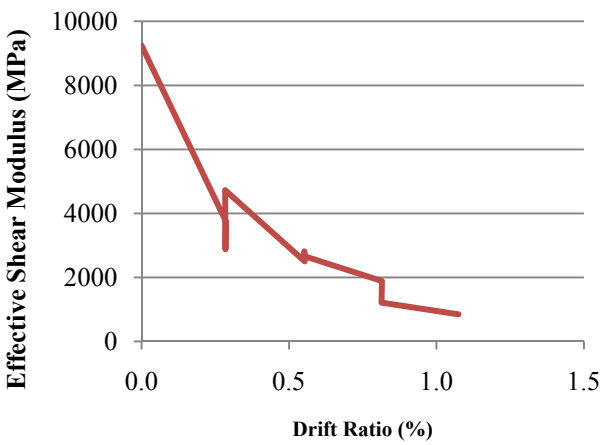

Figure 5. Effective shear modulus for column 3.

caused the control system to detect a reduction in axial load capacity and transition to displacement control in the vertical direction, stabilizing the column at an axial load of 1415 KN. In this case no attempt was made to load the column with the load of 1510 KN, and the displacement of the column resumed with a reduced axial load of 1335 KN. As shown in Fig. 4b, the appearance of the inclined crack caused a significant reduction in lateral stiffness, although unlike in the case of column 1, the lateral stiffness was not completely lost. Subsequent cycles at the reduced axial load of 1335 KN continued until the lateral stiffness was completely lost and a second axial failure event took place after the column had reached a maximum drift ratio of 2%.

The response of column 3, with the higher axial load and longitudinal reinforcement ratio, was the least brittle of the three. As previously indicated, a shear crack through the middle section of the specimen (similar to the shear crack observed in column 2) formed at a drift ratio of 1.07%. In this case the column was able to sustain the full axial load after the shear crack formed, although there was a significant reduction in lateral stiffness with increased lateral deformation. The loading protocol continued and axial failure was observed after the lateral stiffness was completely lost, when the column had reached a maximum drift ratio of 1.58%. Loading resumed at a reduced axial load of 1780 KN, and multiple axial failure events occurred within the same load cycle, with the load eventually stabilizing at a residual value of 668 KN (30% of the initial value and approximately equal to the axial capacity of the longitudinal reinforcement $A_s f_y$).

Figure 4c shows the relationship between the mean axial strain (vertical deformation divided by column height) and axial force for the three column specimens. Columns 1 and 2, with similar reinforcement details but different axial loads, followed a similar axial strain vs. axial load envelope, even though the axial loads were different and the rate at which axial load was lost in the columns was also different. In the case of column 2, a stable plateau was found after the first failure event at an axial load of 1335 KN. Upon subsequent loading, lateral deformations caused damage to the concrete and consequently caused a progressive increase in axial strain. When the axial strain reached the failure envelope at an axial strain of approximately 0.3%, axial failure took place for a second time, approximately following the same axial strain-axial force failure surface observed for column 1.

When comparing the behavior of columns 1 and 3 in Fig. 4d (same axial load with different longitudinal reinforcement ratios) it observed that while column 1 (with a longitudinal reinforcement ratio of 2.5%) experienced axial failure when the shear crack formed and the mean axial strain was 0.13%, column 3 (with a longitudinal reinforcement ratio of 3%) was able to

sustain the axial load past the point of shear failure until the mean axial strain was 0.3%, by far the highest axial deformation of the three columns.

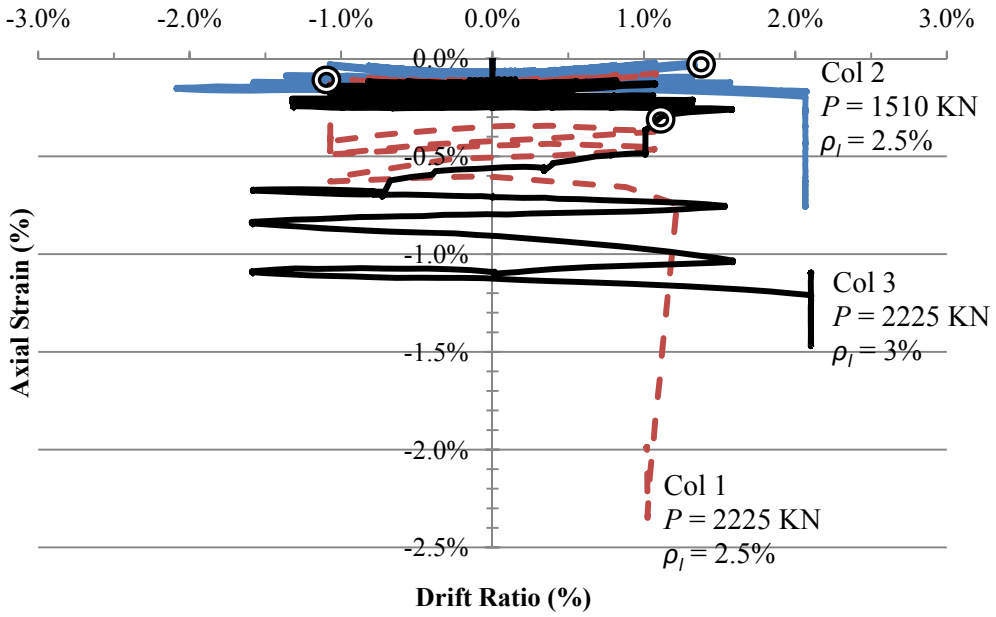

Figure 6. Mean Axial Strain vs. Drift Ratio for Columns 1 through 3.

These readings indicate that the larger amount of longitudinal reinforcement allowed the column to sustain significantly greater damage to the concrete in the core before axial load failure took place. This is also illustrated in Fig. 6, which shows the relationship between mean axial strain and drift ratio for the three columns. A circular marker shows the point at which axial failure was first observed. Figure 6 shows that for all three columns there is an initial region in which the mean axial strain increases with reverse cyclic loading in a stable manner. For column 3, the appearance of a large inclined crack at approximately 1% lateral drift ratio lead to axial failure which is shown by a significant instantaneous increase in mean axial strain, from 0.13% to 0.5%. In the case of column 3, the appearance of the inclined crack through the center region of the column lead to a significant increase in the mean axial strain during the following displacement cycle, from approximately 0.15% to 0.2%. From that point forward, the rate of increase in axial strain with each displacement cycle increased considerably leading to failure at an axial strain of approximately 0.3%. A similar, although less pronounced, type of behavior was observed for specimen 2. The rate of increase of the axial strain with each displacement cycle increased significantly after the shear crack appeared.

Based on these three experiments it is concluded that the rate of increase in axial strain with each displacement cycle was affected by the longitudinal reinforcement ratio and the axial load on the column, with the latter being the parameter with the larger influence on the progression of damage to the core.

Drift at Axial Failure According to Elwood-Moehle Model

Elwood and Moehle (2003) proposed the following equation to calculate the drift at axial

failure based on a shear friction model:

$$\delta = \frac{4}{100} \frac{1 + \tan^2 \theta}{\tan \theta + P\left(\frac{s}{A_{st} f_{yt} d_c \tan \theta}\right)} \quad (1)$$

In Eq. 1 Elwood suggests using an angle of inclination for the shear crack of 65 deg. based on empirical observations from tests performed by Lynn (2001) and Sezen (2000). As Eq. 1 indicates, the Elwood-Moehle model suggests that lateral drift ratio δ at axial failure is inversely proportional to both the applied axial load P and the spacing of the transverse reinforcement s, and directly related to the amount of transverse reinforcement A_{st}.

Figure 7 shows the drift at axial failure for the three column specimens. Successive axial failure events for each column are shown by the markers and the progression for each column is traced by the respective dashed line. Figure 7 also shows that the Elwood-Moehle model resulted in very accurate estimates of the drift ratio at axial failure of columns 1 and 2, which had a longitudinal reinforcement ratio of 2.5% and different values of axial load. It is important to note that the Elwood-Moehle model was calibrated on the basis of columns in which the flexural reinforcement yielded in tension prior to shear failure, which was not the case for columns 1 and 2. In the case of column 3, Fig. 7 shows that the larger longitudinal reinforcement ratio of 3% not only changed the mode of failure of the column, but also provided increased toughness, reflected by a drift ratio at axial failure that was approximately 50% higher than that of column 1.

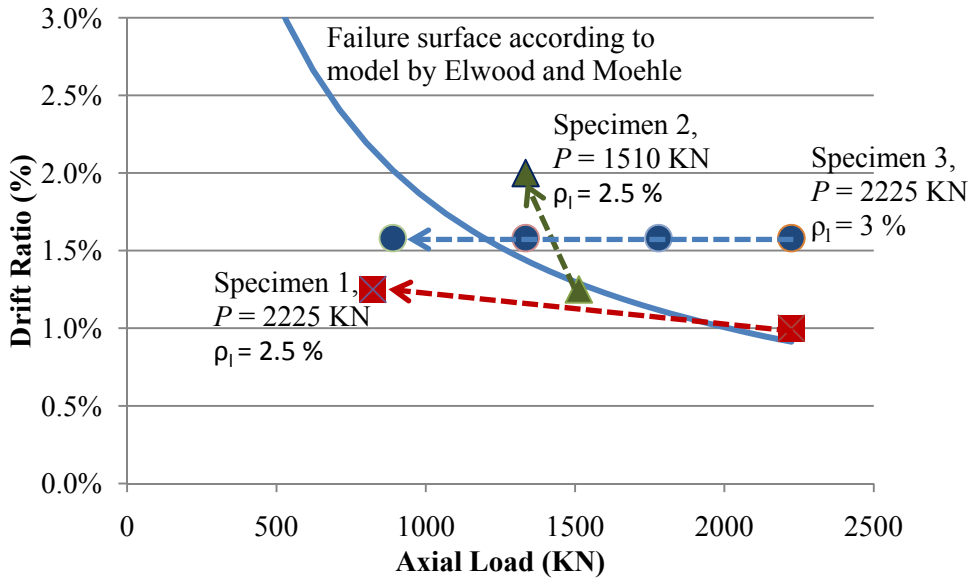

Figure 7. Drift Ratio at axial failure for columns 1 through 3.

The rate at which the axial load capacity was lost after axial failure was similar for columns 1 and 3, and significantly different for column 2. While column 1 transitioned from being able to sustain the full axial load to its residual axial load capacity in one failure event, in column 3 the transition took place progressively over 3 failure events. This difference is in part related to the settings of the control system. After the test of column 1 a much shorter trigger criteria was established for

detecting axial failure events in order to avoid excessive damage to the column. Even though the loss in axial load capacity of column 3 was much more progressive, it occurred within the set of cycles with a maximum drift ratio of 1.5%, with most of the axial failure events occurring within the same unloading cycle. In the two columns with the highest axial load the axial load capacity was lost in a sudden manner. In the case of column 2 the behavior was significantly different, with the column being able to sustain a significantly larger drift demand under reduced axial load after the first failure event. The results from this test suggest than in columns with lower axial loads the loss in axial load capacity occurs in a more gradual manner, likely because the ratio of axial load to buckling capacity of the longitudinal reinforcement allows for redistribution of the axial force between the two materials.

Conclusions

Even though columns 1 and 2 were shear critical and subjected to a very high axial load, estimates of drift ratio at axial failure obtained with the Elwood-Moehle model were accurate. Because this model provides the basis for the ASCE-41 provisions, the load-displacement envelope calculated with supplement 1 resulted in a conservative estimate of the hysteretic response of the column. Shear strength values calculated with the ASCE-41 provisions were conservative, although this was the case also for estimates obtained with the ACI 318 design provisions and the Modified Compression Field Theory. In the case of specimen 3, with a longitudinal reinforcement ratio of 3%, the estimate of the drift at axial failure obtained with the Elwood-Moehle model was significantly conservative, and so was the load-displacement envelope obtained with ASCE-41 supplement 1. Data from the tests suggest that the residual capacity of the columns after axial failure is affected by the level of axial load in the column. Column 2, with lower axial load, had the ability to carry a reduced axial load at drift ratios higher than the drift at axial failure, which was not the case for columns 1 and 3. It is noted that the control settings were adjusted after the first test (column 1), which resulted in lesser damage to columns 2 and 3 during each axial failure event. These results suggest that columns with high axial load pose a greater risk for sudden collapse after axial failure of a column. Conversely, in structures in which the columns have low axial load demands, test results suggests that it may be possible for the column to redistribute a fraction of the axial load through the floor system after axial failure and continue to deform while sustaining a reduced axial load demand.

Acknowledgments

The authors would like to acknowledge the support provided by the staff from the NEES MAST facility at the University of Minnesota. Our thanks to Carol Shield, Paul Bergson, Angela Kingsley, Jonathan Messier and Drew Daugherty for their contributions to make this a successful testing program. The work of Travis Malone, Emily Reimer and Vinur Kaul was instrumental to the successful fabrication of the specimens. Kurt Henkhaus and Julio Ramirez from Purdue University provided valuable feedback and were actively involved during the planning, instrumentation, and testing of the specimens. Their valuable contributions are gratefully acknowledged. This work was supported primarily by the National Science Foundation under award number # 0618804 through the Pacific Earthquake Engineering Research Center (PEER). Any opinions, findings, and conclusions or recommendations expressed in this material are those of the author(s) and do not necessarily reflect those of the National Science Foundation.

References

ACI Committee 318, 2008. Building Code Requirements for Structural Concrete and Commentary. American Concrete Institute, Farmington Hills, MI. 467 pp.

Bentz, E., and Collins, M., 2000. Response 2000, Reinforced Concrete Sectional Analysis using the Modified Compression Field Theory, University of Toronto, http://www.ecf.utoronto.ca/~bentz/home.shtml

Elwood, Kenneth J. and Jack P. Meohle. 2003. "Shake Table Tests and Analytical Studies on the Gravity Load Collapse of Reinforced Concrete Frames". *PEER Report 2003/01*, Pacific Earthquake Engineering Research Center, University of California, Berkeley, 346 pp.

Elwood, Kenneth J., et al., 2007. "Update to ASCE/SEI 41 Concrete Provisions". *Earthquake Spectra*. 23, (3), pp. 493-523.

Lynn, Abraham C., 2001, "Seismic Evaluation of Existing Reinforced Concrete Building Columns". *PhD Dissertation*, University of California, Berkeley.

Matchulat, L., 2008. "Mitigation of Collapse Risk in Vulnerable Concrete Buildings." *MS Thesis*, University of Kansas.

Sezen, Halil., 2000, "Seismic Behavior and Modeling of Reinforced Concrete Building Columns". *PhD Dissertation*, University of California, Berkeley.